Supplementary Information:

Order from a Mess: The Growth of 5-Armchair Graphene Nanoribbons

Alejandro Berdonces-Layunta,[1,2,†] Fabian Schulz,[3,4,†,*] Fernando Aguilar-Galindo,[1,†] James Lawrence,[1,2] Mohammed S. G. Mohammed,[1,2] Matthias Muntwiler,[5] Jorge Lobo-Checa,[6,7] Peter Liljeroth,[3] Dimas G. de Oteyza.[1,2,8,*]

[1] Donostia International Physics Center, 20018 San Sebastián, Spain

[2] Centro de Física de Materiales, 20018 San Sebastián, Spain

[3] Department of Applied Physics, Aalto University, FI-00076 Aalto, Finland

[4] Fritz Haber Institute of the Max Planck Society, 14195 Berlin, Germany

[5] Paul Scherrer Institute, 5232 Villigen, Switzerland

[6] Instituto de Nanociencia y Materiales de Aragón, 50009 Zaragoza, Spain

[7] Dpto. de Física de la Materia Condensada, Universidad de Zaragoza, 50009 Zaragoza, Spain

[8] Ikerbasque, Basque Foundation for Science, 48009 Bilbao, Spain

† these authors contributed equally

* correspondence to: schulz@fhi-berlin.mpg.de, d_g_oteyza@ehu.es

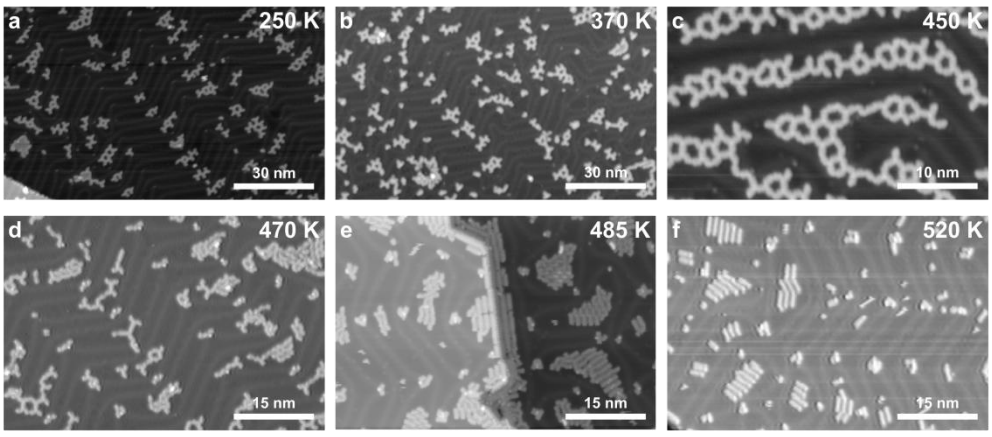

Fig. S1. STM overview images of the DBP/Au(111) sample after annealing to various temperatures. STM set points as indicated. (a) Low coverage of DBP on Au(111) as-deposited at 250 K (-1.05 V, 0.1 nA). (b) The sample of Fig. S1a in the main manuscript after annealing to 100 °C (0.30 V, 0.20 nA). (c) The sample of Fig. 2a in the main manuscript after annealing to 175 °C (-0.78 V, 0.12 nA). (d) After annealing to 200 °C (0.48 V, 0.33 nA). (e) After annealing to 215 °C (-0.95 V, 0.05 nA). (f) After annealing to 250 °C (-0.58 V, 0.07 nA).

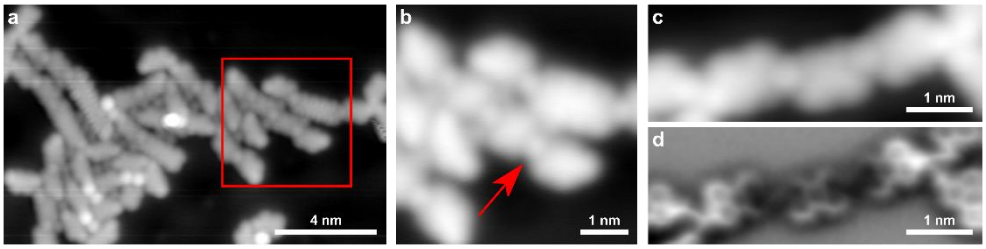

Fig. S2. Coexistence of all reaction species. STM and AFM set points as indicated. (a) STM image of a typical molecular aggregate observed after annealing DBP/Au(111) to 200 °C (-0.22 V, 0.08 nA). (b) Corresponding STM image (region marked with a red square in panel a) of the AFM image in Fig. 2d in the main manuscript (1.31 V, 0.10 nA). The red arrow marks a circular feature linking two (partially) debrominated DBP monomers. (c, d) Corresponding STM and AFM image of the Laplace-filtered AFM image in Fig. 2e, respectively (0.20 V, 0.10 nA, Δz = 0.2 Å).

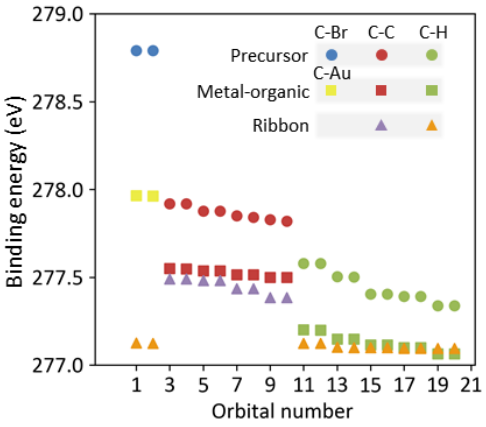

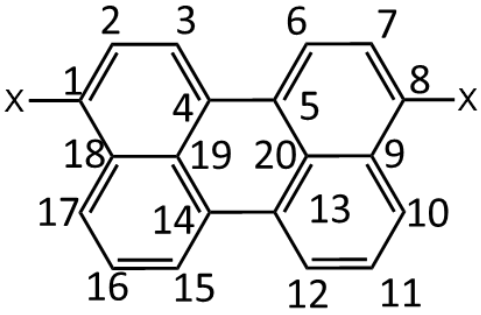

	Different carbons taking part in the orbital		
# orbital	**Precursor X=Br**	**MO X=Au**	**Ribbon X=H**
1	1, 10	1, 10	1, 3, 6, 8, 10, 12, 15, 17
2	1, 10	1, 10	1, 3, 6, 8, 10, 12, 15, 17
3	9, 18	9, 18, 19, 20	4, 5, 14, 13
4	9, 18	9, 18, 19, 20	4, 5, 14, 13
5	19, 20	9, 18, 19, 20	4, 5, 14, 13
6	19, 20	9, 18, 19, 20	4, 5, 14, 13
7	4, 5, 13, 14	4, 5, 13, 14	19, 20
8	4, 5, 13, 14	4, 5, 13, 14	19, 20
9	4, 5, 13, 14	4, 5, 13, 14	9, 18
10	4, 5, 13, 14	4, 5, 13, 14	9, 18
11	2, 11	2, 11	2, 7, 11, 16
12	2, 11	2, 11	2, 7, 11, 16
13	3, 12	3, 12	2, 7, 11, 16
14	3, 12	3, 12	2, 7, 11, 16
15	6, 7, 15, 16	6, 7, 15, 16	1, 3, 6, 8, 10, 12, 15, 17
16	6, 7, 15, 16	6, 7, 15, 16	1, 3, 6, 8, 10, 12, 15, 17
17	6, 7, 15, 16	6, 7, 15, 16	1, 3, 6, 8, 10, 12, 15, 17
18	6, 7, 15, 16	6, 7, 15, 16	1, 3, 6, 8, 10, 12, 15, 17
19	8, 17	8, 17	1, 3, 6, 8, 10, 12, 15, 17
20	8, 17	8, 17	1, 3, 6, 8, 10, 12, 15, 17

Fig. S3. Due to the symmetry of the molecules, the energy of the calculated orbitals are often associated to more than one carbon atom. The additional list displays the correspondence between every orbital for each species shown in the graph with a group of carbons of the precursor, intermediate or product.

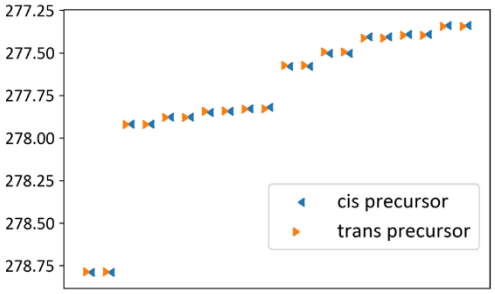

Fig. S4. C1s XPS simulations for the two racemates of the precursor.

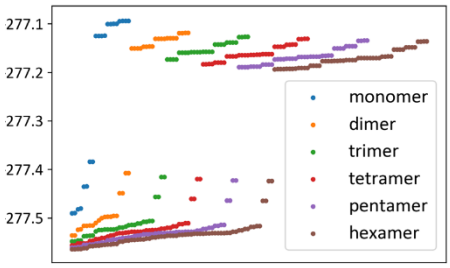

Fig S5. C1s XPS simulations for different ribbon lengths. Note how the carbons energetically split in two separate groups: C-C and C-H. The four signals around 277.4 eV that stand out belong to the carbons of the zigzag edge.

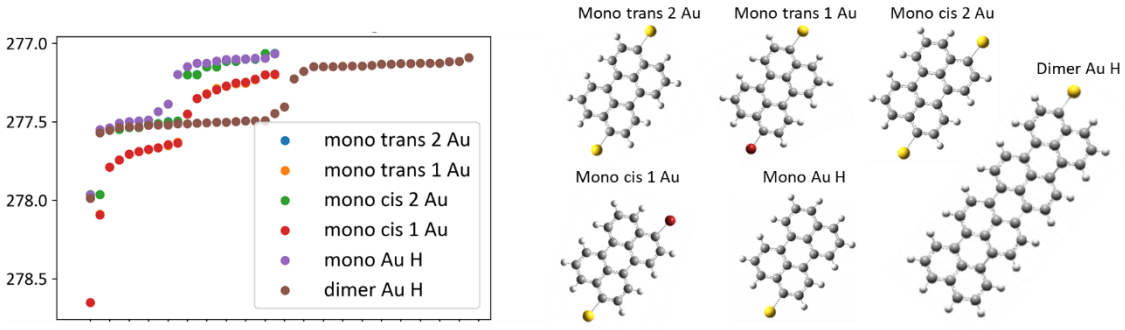

Fig S6. C1s XPS simulations for the different types of MO observed in the AFM images.

Supplementary note 1. C1s XPS: analysis and interpretation

The starting considerations include our experimental observation of a metal-organic intermediate within a limited temperature range. However, as readily extracted from our SPM experiments, even within the right temperature window the number of molecules forming the metal-organic intermediate is limited, coexisting with the other molecular species. Since only two atoms per precursor molecule coordinate at most to metal atoms, the stoichiometric ratio of these carbon species is extremely limited throughout the whole growth process.

Below we describe the different approaches that have been followed to fit the C1s spectra.

First approach: Precursor and ribbons.

As a starting point, we have fitted the spectra associated to as-deposited molecules and to the GNRs, as extracted from the first and last spectra during our temperature ramp.

For the as-deposited molecules the carbon signal was modelled with three components based on theoretical core level energy calculations. The carbons bonded to hydrogen (C-H) are the lowest in energy. Then, the fully substituted inner Carbons (C-C). The highest binding energy is displayed by those carbons attached to Br (C-Br). The ratio between the components was fixed according to the molecule's stoichiometry (C-H)/(C-C)/(C-Br) = 10/8/2. Parameters like shape, Full-Width Half Minimum (FWHM), relative and absolute position of the peaks were optimized to get the best possible fit. The resulting fit provides notable differences in the FWHM of each of the components, which are in qualitative agreement with the energy spread theoretically predicted for the core levels within each group (see Fig. 4c in main text).

For the GNRs the calculations predict two different groups of carbons, one for the external C-H carbons and one for the internal ones. In this case, the ratio C-C/C-H depends on the average length of the fully grown GNRs according to $= \frac{12N-4}{8N+4}$; where *N* is the number of precursor units.

As a result, we can estimate the average ribbon length from the fitted C-C/C-H ratio.

In spite of the highly asymmetric line shape of the spectra, each of the fitting components is maintained symmetric. Although asymmetric peaks have been used in the study of GNRs earlier, we believe that their use is not really justified here, because the bandgap of these GNRs prevents the low energy excitations that are normally imposed to justify the high binding energy "tails" of the core level peaks.

Within our first approach, the fitting of all spectra consisted in a linear combination of the components associated to reactants and to GNRs. In Fig. S6 we include sample spectra for the two reference situations, along with a list of the free and fixed parameters that the system could modify.

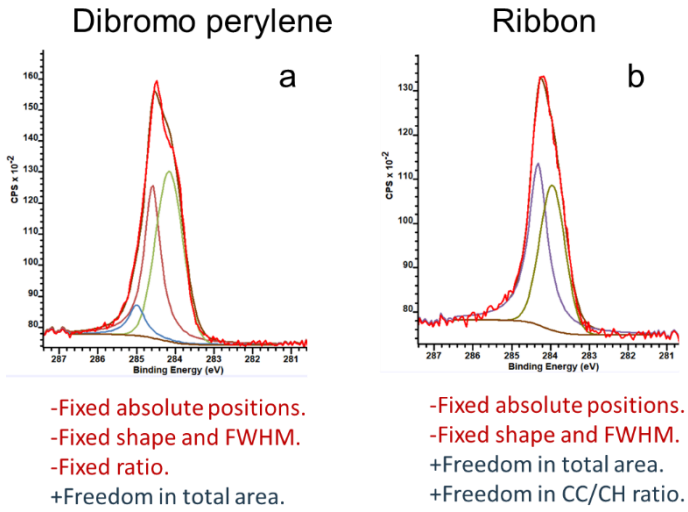

Fig. S7. Sample spectra for the two reference situations, namely as-deposited molecules (a) and GNRs (b), along with the parameters that have been fixed and fitted for the various components, respectively.

With these three degrees of freedom, the resulting fit seemed to follow the expected tendency. However, two main problems arise:

-The temperature window of active reactivity is poorly fitted, in particular at the low binding energy side (See Fig. S8).

-The ratio between the peaks of the ribbon exceeds the limits (C-C/C-H) = 0.66 ≤ r ≤1.5.

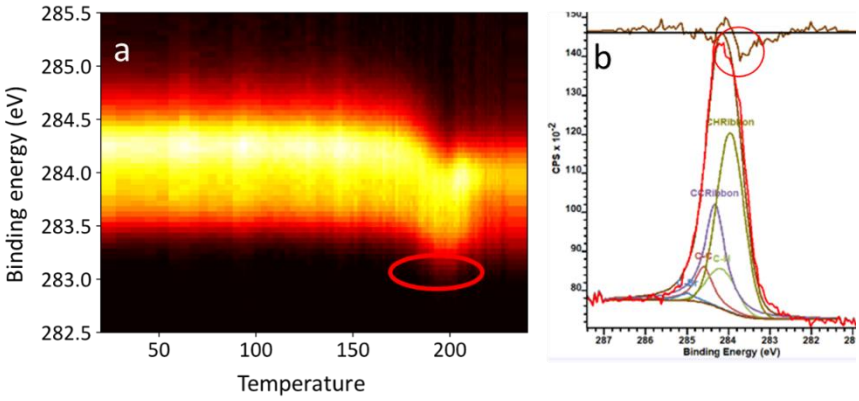

Fig. S8. The first fitting approach failed in addressing the XPS signal under 284 eV. It caused a systematic error and an unphysical C-C/C-H ratio.

Second approach: Addition of the metal-organic.

To overcome the inconsistencies obtained from the previous fitting approach, we tried adding the metal-organic signal to fill the gaps left by the other two compounds. The signal associated to DBP and ribbons, as fitted in the first and last spectra, is maintained. For the metal-organic, we employed the less reliably fit spectra from the previous approach, which was assumed to contain the largest metal-organic contribution.

The relative energies for the C-C/C-H components of the metal-organic molecules have been maintained as in the previous cases. A lower binding energy for a metal-organic may be justified by a significant inductive effect caused by the Au atom. To be consequent, we placed the coordinated carbon peak (C-Au) at lower binding energies, as the literature conventionally does for the other coinage metals (Ag, Cu), although contradicting the core level energies obtained from our DFT calculations (Fig. 4c).

Representative sample spectra of the three different scenarios during the temperature ramp are displayed in Fig. S8, along with the parameters that are fitted or fixed, respectively.

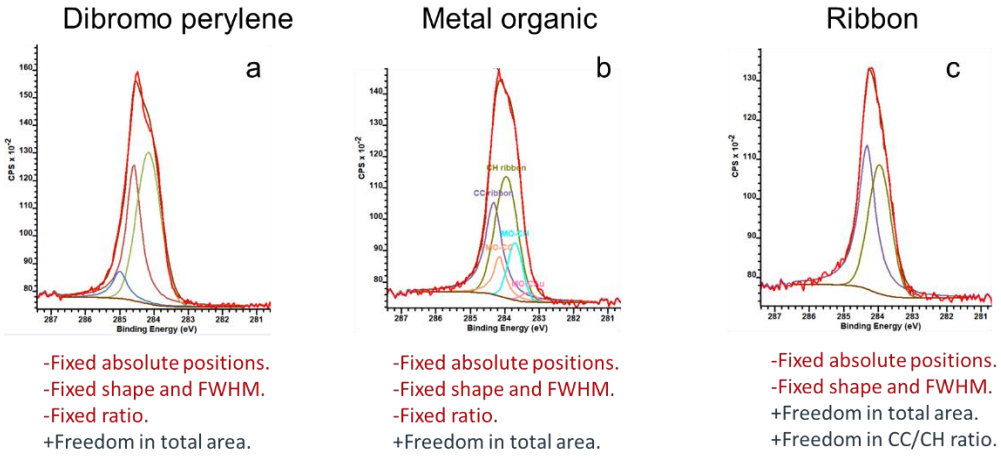

Fig. S9. Degrees of freedom and conditions of the new fitting.

With this new variable, the fitting improves, but the temperature-dependent amount of each component (Fig. S10) shows an unreasonable evolution with the (metal-organic) intermediate, since it maximizes with the (GNR) final product, instead of before. We therefore also discarded these fitting results.

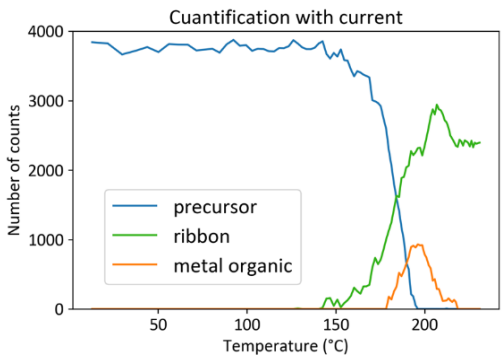

Fig. S10 Temperature-dependent evolution of the relative amounts of as-deposited, metal-organic and GNR molecules, as obtained within this second fitting approach including the metal-organic species.

Third approach: Addition of the Br-associated work function modulation.

The discrepancies on the low binding energy side obtained with our first fitting approach (Fig. S7) may also be an effect of the atomic Br on the local work function. In a new approach, we proceed fitting with a linear combination of as-deposited molecules and GNRs, in combination with a work function modulation that correlates with the concentration of atomic Br on the metal surface. Such optimal fitting result corrected the inconsistencies or deficiencies from the previous two approaches.

We estimate the shift in the local work function analyzing the DBP Br signal, which displays the following advantages: it is associated with unchanged molecules and can therefore be associated to work function modifications, it can be followed univocally along the reaction and, being bound to the molecular carbon backbone, the effect on the carbon atoms can be assumed to be similar. Figure S11a shows the rigid shift of the DBP Br doublet during the temperature ramp, whereas Fig. S11b shows its linear correlation with the concentration of atomic Br on the surface. With this correlation at hand, we can estimate the associated shift of the carbon core levels throughout the temperature ramp, as plotted in Fig. S11c, and apply it to the fitting of the temperature-dependent spectra.

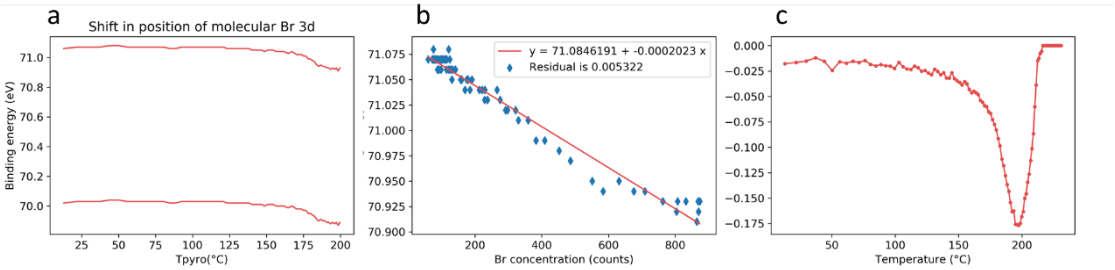

Fig. S11. a) Position of the pairs of bromine peaks with the temperature. Although the atomic Br peak shifts dramatically, the effect is also observed in the molecular Br. It has been proposed previously that the presence of atomic Br in the surface can change the average work function. b) Linear correlation between the Br concentration and the binding energy shift of the molecular Br. c) Estimated shift of the carbon XPS, as extracted from applying the function of b) to the atomic Br concentration.

Supplementary note 2. Optimized geometries (xyz coordinates, Å) and absolute Gibbs free energies of the different products.

a) Linear coupling product.

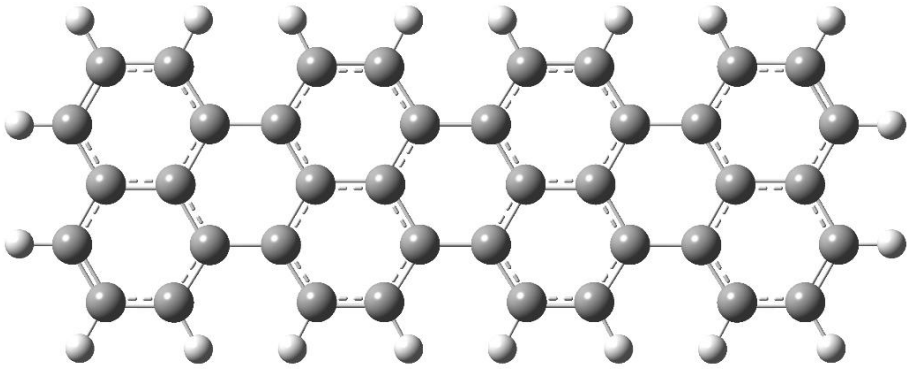

Gibbs free energy (a.u.): -1536.114896

C	-1.47336100	-2.42392200	-0.00001200
C	-0.73366200	-1.23815600	-0.00001300
C	-1.45281000	-0.00006100	-0.00001200
C	-2.89488300	-0.00004200	-0.00000700
C	-3.60949600	-1.24206400	0.00001200
C	-2.86673600	-2.42443600	0.00000100
H	-0.96735400	-3.38830300	-0.00002100
C	-0.73365600	1.23802800	-0.00001700
C	-3.60945000	1.24201100	-0.00002300
H	-3.37184500	-3.38947900	-0.00000100
C	-2.86667300	2.42436600	-0.00003100
C	-1.47329600	2.42381400	-0.00002600
H	-3.37176800	3.38941900	-0.00003900
H	-0.96723500	3.38817700	-0.00003000
C	-5.08131200	1.24730900	-0.00003400
C	-5.78750600	0.00001800	0.00000600
C	-5.82193900	2.43155700	-0.00007900
C	-5.08136500	-1.24730500	0.00004100
C	-7.22437800	0.00005800	0.00001500
C	-7.22912800	2.42763800	-0.00007800
H	-5.31431500	3.39536400	-0.00011800
C	-5.82206700	-2.43151200	0.00009900
C	-7.92368200	-1.23585600	0.00006800
C	-7.92361600	1.23601200	-0.00002900
H	-7.76576900	3.37882000	-0.00011500
C	-7.22925500	-2.42751800	0.00011300
H	-5.31451000	-3.39535100	0.00013900
H	-9.01610800	-1.22403000	0.00007400
H	-9.01604200	1.22423800	-0.00002500
H	-7.76594900	-3.37867000	0.00015900
C	0.73364700	1.23802900	-0.00001200
C	1.47328100	2.42382200	-0.00001000
C	1.45281000	-0.00005100	-0.00001100
C	2.86665600	2.42438400	0.00000200
H	0.96721000	3.38817900	-0.00001800
C	2.89488300	-0.00001800	-0.00000700
C	0.73367000	-1.23815400	-0.00001700
C	3.60945200	1.24203400	0.00001200
H	3.37173100	3.38944400	0.00000100
C	3.60949400	-1.24204100	-0.00002300
C	1.47337600	-2.42391400	-0.00002400
C	5.08132100	1.24732500	0.00004100
C	2.86675300	-2.42441800	-0.00002900
C	5.08135600	-1.24729000	-0.00003400
H	0.96737900	-3.38830000	-0.00002800
C	5.78750600	0.00002800	0.00000700
C	5.82197700	2.43156100	0.00009900
H	3.37188100	-3.38945300	-0.00003600
C	5.82202800	-2.43150800	-0.00008000
C	7.22437800	0.00004300	0.00001400
C	7.22916500	2.42761900	0.00011200
H	5.31438200	3.39537900	0.00013900
C	7.22921800	-2.42753700	-0.00007900
H	5.31444300	-3.39533600	-0.00011800
C	7.92363600	1.23598200	0.00006700
C	7.92366200	-1.23588600	-0.00003000
H	7.76582400	3.37879100	0.00015800
H	7.76589300	-3.37869900	-0.00011600
H	9.01606200	1.22419700	0.00007300
H	9.01608800	-1.22407200	-0.00002500

b) Kinked product.

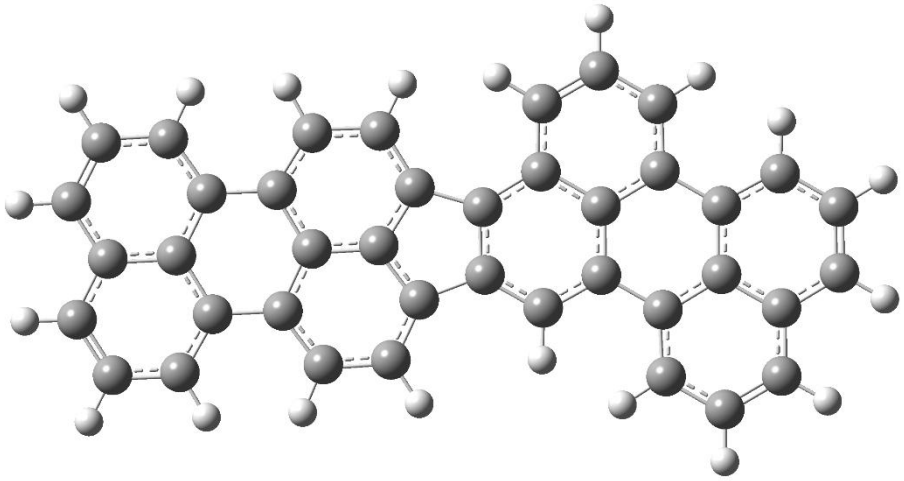

Gibbs free energy (a.u.): -1536.097849

C	0.65927100	-0.59622500	0.00003400
C	0.61268000	0.81793800	0.00004000
C	1.83030100	1.55771200	0.00005100
C	3.08458000	0.83750200	0.00002900
C	3.09413500	-0.60071000	0.00003700
C	1.87653300	-1.28423700	0.00003500
H	0.91373300	3.52704600	0.00013400
C	1.85208000	2.97724600	0.00009100
C	4.31716400	1.57545500	0.00000400
H	1.85547600	-2.37333800	0.00002700
C	4.26780500	2.96851200	0.00004300
C	3.04693300	3.66412800	0.00009300
H	5.18842400	3.55014200	0.00004200
H	3.05150200	4.75619900	0.00013400
C	5.60604200	0.85025000	-0.00006200
C	5.60747500	-0.58284000	-0.00002200
C	6.83161000	1.51592700	-0.00016100
C	4.38018300	-1.32501800	0.00004800
C	6.85970600	-1.28816400	-0.00005100
C	8.05702100	0.82207900	-0.00020400
H	6.86397800	2.60461600	-0.00021100
C	4.44755100	-2.71877300	0.00012200
C	6.86470200	-2.70826300	0.00001400
C	8.07630600	-0.55588500	-0.00014300
H	8.99133000	1.38762900	-0.00028200
C	5.67625100	-3.40620300	0.00010600
H	3.53392500	-3.31166900	0.00019600
H	7.82300200	-3.23284900	-0.00000600
H	9.02176100	-1.10333900	-0.00016800
H	5.67721800	-4.49834400	0.00016500
C	-0.80654200	1.22464400	0.00003100
C	-1.53848700	2.40866300	0.00002900
C	-1.56162300	0.01725900	0.00001600
C	-2.95328100	2.36513900	0.00001700
H	-1.06275200	3.38941000	0.00003100
C	-2.95883800	-0.05358300	0.00000500
C	-0.71592700	-1.11667300	0.00001300
C	-3.69170200	1.17410100	0.00000300
H	-3.47707300	3.32154700	0.00001900
C	-3.56553900	-1.34968500	-0.00000200
C	-1.30806500	-2.37020800	0.00000400
C	-5.16046800	1.09963100	-0.00001200
C	-2.72011900	-2.46851400	-0.00000200
C	-5.03634100	-1.41756300	-0.00000800
H	-0.71355700	-3.28694200	0.00000500
C	-5.79407200	-0.19330400	-0.00001300
C	-5.96184900	2.24067400	-0.00002900
H	-3.15249900	-3.46941700	-0.00000400
C	-5.72243300	-2.63124600	-0.00001100
C	-7.22861900	-0.26364200	-0.00002100
C	-7.36751400	2.16295900	-0.00003800
H	-5.49836200	3.22741000	-0.00003800
C	-7.12907500	-2.69182000	-0.00001600
H	-5.16518700	-3.56815500	-0.00001100
C	-7.99297900	0.93422700	-0.00003200
C	-7.87203600	-1.53052200	-0.00002100
H	-7.95617800	3.08267200	-0.00005000
H	-7.62453500	-3.66491500	-0.00001800
H	-9.08313500	0.86237600	-0.00003700
H	-8.96399100	-1.56588000	-0.00002600

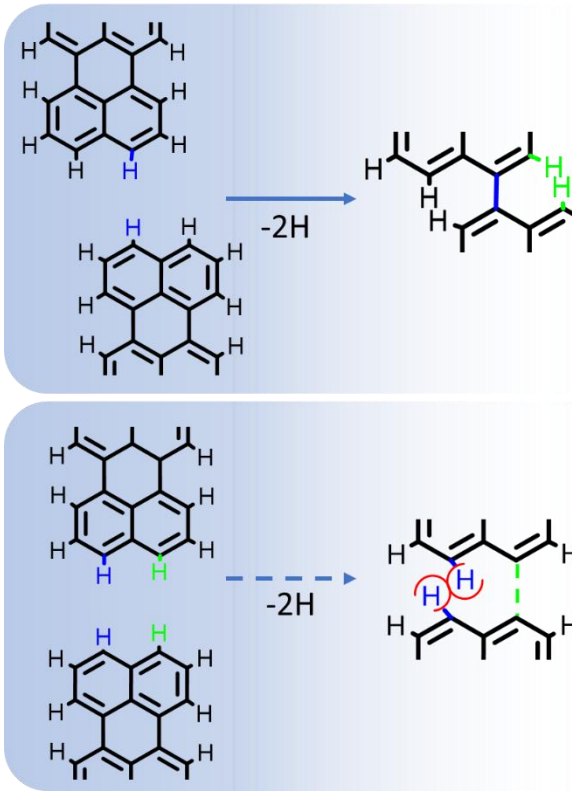

Fig. S12. Proposed mechanism for the halogen-free molecular coupling. There is an expected two-step mediated reaction. With submonolayer coverages, the reaction is regioselective towards their kinked fusion (a), kinetically determined due to the steric hindrance in the straight reaction pathway (b).